Identification of dendritic antigen-presenting cells in the zebrafish

Geanncarlo Lugo-Villarino[a,1], Keir M. Balla[a,1], David L. Stachura[a], Karina Bañuelos[a], Miriam B. F. Werneck[b], and David Traver[a,c,2]

[a]Section of Cell and Developmental Biology, Division of Biological Sciences, University of California, La Jolla, CA 92093-0380; [b]Division of Cellular Biology, Brazilian National Cancer Institute (INCA), Rio de Janeiro, 22031-050, Brazil; and [c]Department of Cellular and Molecular Medicine, University of California, La Jolla, CA 92093-0380

Edited* by Laurie H. Glimcher, Harvard University, Boston, MA, and approved June 2, 2010 (received for review January 13, 2010)

In mammals, dendritic cells (DCs) form the key link between the innate and adaptive immune systems. DCs act as immune sentries in various tissues and, upon encountering pathogen, engulf and traffic foreign antigen to secondary lymphoid tissues, stimulating antigen-specific T lymphocytes. Although DCs are of fundamental importance in orchestrating the mammalian immune response, their presence and function in nonmammalian vertebrates is largely unknown. Because teleosts possess one of the earliest recognizable adaptive immune systems, we sought to identify antigen-presenting cells (APCs) in the zebrafish to better understand the potential origins of DCs and their evolutionary relationship to lymphocytes. Here we present the identification and characterization of a zebrafish APC subset strongly resembling mammalian DCs. Rare DCs are present in various adult tissues, and can be enriched by their affinity for the lectin peanut agglutinin (PNA). We show that PNA^{hi} myeloid cells possess the classical morphological features of mammalian DCs as revealed by histochemical and ultrastructural analyses, phagocytose-labeled bacterial preparations in vivo, and exhibit expression of genes associated with DC function and antigen presentation, including *il12*, MHC class II invariant chain *iclp1*, and *csf1r*. Importantly, we show that PNA^{hi} cells can activate T lymphocytes in an antigen-dependent manner. Together, these studies suggest that the cellular constituents responsible for antigen presentation are remarkably conserved from teleosts to mammals, and indicate that the zebrafish may serve as a unique model to study the origin of APC subsets and their evolutionary role as the link between the innate and adaptive immune systems.

dendritic cells | peanut agglutinin | keyhole limpet hemocyanin | IL-12

In 1868, Paul Langerhans made the first description of dendritic cells (DCs) found in human skin that he regarded as "intra-epidermal receptors for extracutaneous signals of the nervous system" (1). Over a century later, this DC subset bearing his name, the Langerhans cell (LC), remained an enigma to dermatologists. It was not until the 1970s that Steinman and Cohn clearly identified the DC as a distinct cell type with unique morphology, tissue distribution, cell-surface phenotype, and function (2–5). Seminal studies using purified DCs demonstrated their ability to induce T-cell activation and proliferation, establishing their role as "professional" APCs (6). In the interim, the role of DCs in regulating microbial infections, cancer, and autoimmune disorders is increasingly being recognized.

Since the first descriptions of DCs in humans and mice, this cell type has been identified in other mammals, birds, reptiles and amphibians, but not in fish (7). In evolutionary terms, teleosts possess one of the earliest recognizable adaptive immune systems, containing B and T lymphocytes with somatically rearranged antigen receptors, the major histocompatibility complex (MHC), and immunological memory (8, 9). Therefore, the presence of DCs in bony fish would provide key information regarding the ontogeny of specific immunity in vertebrates. To date, the only evidence supporting the existence of DCs in vertebrate fish comes from the morphological description of Birbeck granules, a unique feature of mammalian LCs, in leukocytes from lymphoid tissues of salmonids and from inflammatory lesions in rainbow trout bearing microsporidial gill disease (10). Here, we have addressed the biology of DCs in the zebrafish, a small cyprinid teleost that features an immune system similar to that of mammals (11).

Results and Discussion

Identification of DCs in Zebrafish. We previously determined that the major hematopoietic lineages of the zebrafish could be identified by light-scatter characteristics using fluorescence activated cell sorting (FACS) (12). Here, we modified this technique to allow detection of APCs. Because a hallmark of APCs is the phagocytosis of pathogens, we performed i.p. injections of Alexa 488-labeled, heat-killed *Staphylococcus aureus* to identify resident phagocytes. After 16 h, we collected i.p. exudate (IPEX) and assessed phagocytosis by FACS. As shown in Fig. 1*A Center*, 5 ± 1.8% ($n = 11$) of peritoneal cells phagocytosed *S. aureus* (1.1×10^4 ± 962 phagocytes/fish, $n = 6$), and the vast majority of these phagocytes (Alexa 488^+ cells) were present in the light-scatter gate previously shown to contain myelomonocytes in zebrafish (Fig. 1*A Right*, green gate) (12). Fluorescent phagocytes were sorted from the myelomonocyte gate and stained with Wright-Giemsa (WG) to assess cellular morphology. Most phagocytes were neutrophils (40 ± 15.5%), as distinguished by clear cytoplasm and segmented nuclei (Fig. 1*B*, *i*), and monocytes and macrophages (Mφs) (52 ± 12%), characterized by high cytoplasmic-to-nuclear ratios and agranular cytoplasm containing vacuoles (Fig. 1*B*, *ii* and *iii*). Importantly, we identified cells that morphologically resembled mammalian DCs. Over 7 ± 2.5% ($n = 6$) of Alexa 488^+ cells displayed dendritic filaments emanating from the cell body. These dendrites varied in length, width, form, and number, resulting in stellate or elongated cell shapes. Nuclei were oval or kidney shaped, and cytoplasm was devoid of large granules (Fig. 1*B*, *iv–vi*). Together, these findings indicate that the zebrafish immune system includes phagocytes similar to those in mammals, including DC-like cells. Thus, the cellular constituents of the antigen presentation process appear to be well conserved from teleosts to higher vertebrates.

Enrichment of Zebrafish DCs by Flow Cytometry and Lectin-Binding Affinity. Although our in vivo phagocytosis assay allowed us to identify DCs in the zebrafish, this assay did not provide the yield of phagocytes necessary for further characterization of these rare cells. With the zebrafish being a relative newcomer to the field of immunology, there are fewer tools, such as monoclonal anti-

Author contributions: G.L.-V., K.M.B., D.L.S., M.B.F.W., and D.T. designed research; G.L.-V., K.M.B., D.L.S., and K.B. performed research; G.L.-V., K.M.B., D.L.S., and M.B.F.W. contributed new reagents/analytic tools; G.L.-V., K.M.B., D.L.S., M.B.F.W., and D.T. analyzed data; G.L.-V., K.M.B., D.L.S., and D.T. wrote the paper.

The authors declare no conflict of interest.

*This Direct Submission article had a prearranged editor.

[1]G.L.-V. and K.M.B. contributed equally to this work.

[2]To whom correspondence should be addressed. E-mail: dtraver@ucsd.edu.

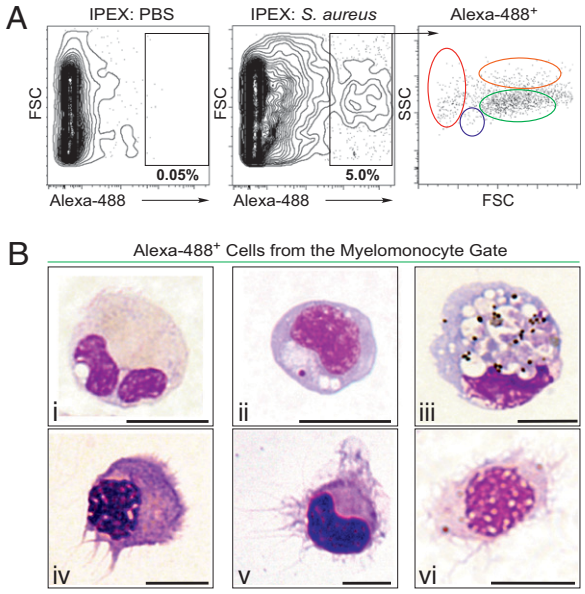

Fig. 1. Identification of DCs in zebrafish. (*A*) PBS (*Left*) or *S. aureus* Alexa 488 (*Center*) was injected i.p., and IPEX cells were collected after 16 h. Phagocytes (black gate, *Center*) were detected by Alexa 488 fluorescence (5.06 ± 1.84%, n = 11) and separated according to their light-scatter characteristics (*Right*) as erythrocytes (red gate), lymphocytes (blue gate), myelomonocytes (green gate), or eosinophils (orange gate). (*B*) IPEX phagocytes within the myelomonocyte gate (green) were isolated ($1.1 \times 10^4 \pm 962$ phagocytes/fish) and subjected to cytospin analysis followed by WG staining. (*Upper*) Phagocytic myelomonocytes, including neutrophils (*i*, 40 ± 15%), monocytes, and Mφs (*ii* and *iii*, 52 ± 12%). (*Lower*) DCs (*iv–vi*, 7 ± 2.5%); n = 6, ± indicates SD. (Scale bar: 5 μm.)

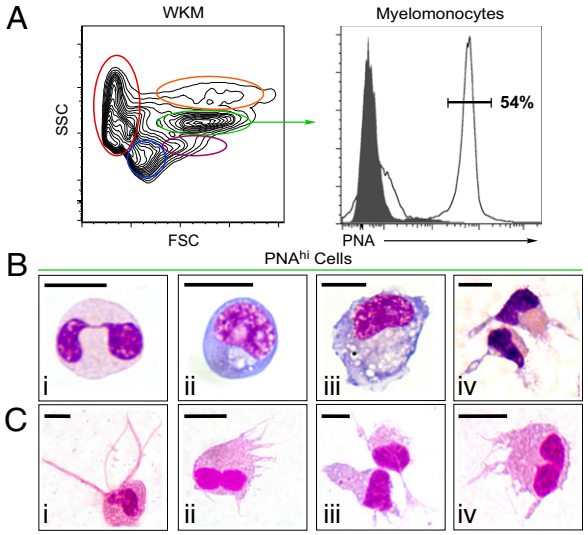

Fig. 2. Enrichment of zebrafish DCs by flow cytometry and lectin-binding affinity. Single-cell suspensions were prepared from WKM and labeled with PNA. (*A*) Contour plot (*Left*) demonstrates the distribution of cells in WKM by light scatter: erythrocytes (red), lymphocytes (blue), precursors (purple), myelomonocytes (green), and eosinophils (orange). Histogram (*Right*) shows PNA binding (black unshaded histogram) and negative control (shaded gray histogram) within the myelomonocyte gate. (*B*) Cytospin analysis of PNA^{hi} myelomonocytes purified from WKM and stained with WG: neutrophils (*i*), monocytes (*ii*), Mφs (*iii*), and DCs (*iv*). (*C*) DC-like cells isolated from other organs and peripheral sites based on PNA binding: skin (*i*), gut (*ii*), IPEX (*iii*), and gills (*iv*). (Scale bar: 5 μm.)

bodies, available to perform prospective isolation techniques (11). Therefore, we sought alternative methods of cellular subfractionation, including differential lectin-binding affinity. Lectins are sugar-binding proteins that recognize complex carbohydrate structures on the cell surface and have been used extensively to distinguish different leukocyte populations in mice and humans (13). Peanut agglutinin (PNA) is a lectin that binds preferentially to galactosyl (β−1, 3) N-acetylgalactosamine, a carbohydrate structure present on some leukocytes, including DC subsets in humans and LCs in both mouse and guinea pigs (14–16). For these reasons, we examined PNA binding on zebrafish leukocytes. We chose whole kidney marrow (WKM) as the source of leukocytes because it contains all major blood cell lineages in abundance (12). Similar to the scarcity of DCs in mammalian tissues, zebrafish DCs were rare ($0.18 \pm 0.1\%, n = 4$) within unfractionated WKM. When cells from WKM are separated based on their light-scatter characteristics by FACS, the vast majority of DC-like cells were found within the myelomonocyte fraction (Fig. 2*A Left*, green gate) and comprised 2.05 ± 0.2% (n = 4) of cells within this population. However, the final yield obtained by light-scatter fractionation is too low ($\approx 2.5 \times 10^4$ myelomonocytes/WKM) after back-to-back sorting to enable the purification of high numbers of DCs. Further fractionation of the myelomonocyte population was achieved using PNA affinity. Whereas just over half of the myelomonocyte fraction (Fig. 2*A Left*, green gate) displayed high PNA affinity (54.3 ± 8.6% PNA^{hi} cells; n = 26; Fig. 2*A Right*), sorting of the PNA^{hi} myelomonocyte fraction yielded a higher number of total cells ($\approx 8.5 \times 10^4$ myelomonocytes/WKM) and an approximate 6-fold enrichment of DCs when compared with purified myelomonocytes alone. Morphological analyses revealed that the majority of purified PNA^{hi} myelomonocytes were neutrophils (60.0 ± 15%, n = 3; Fig. 2*B*, *i*), followed by monocytes (17.5 ± 7.3%, n = 3; Fig. 2*B*, *ii*) and Mφs (10.0 ± 3.5%, n = 3; Fig. 2*B*, *iii*). Importantly, 12.8 ± 2.6% (n = 6) of the PNA^{hi} myelomonocytes displayed morphological features similar to mammalian DCs, including large veils or dendrites extending in several directions from the cell body, stellate or bipolar elongated cell shape, and kidney-shaped nuclei (Fig. 2*B*, *iv*). In addition, we observed high mobility of PNA^{hi} DCs in culture, an important characteristic that distinguishes these cells from other leukocytes in mammals (2, 17). No DCs were found within the PNA^{neg} myelomonocyte fraction. That DCs can be enriched 70-fold over unfractionated WKM using PNA affinity shows that combined light-scatter gating and lectin-binding affinity is useful to identify and isolate DCs from WKM and other immune-related tissues (Fig. 2*C*).

Morphological Characterization of Zebrafish DCs. Historically, the morphology of DCs was characterized in multiple species using various histochemical stains and ultrastructural analyses (7). The ability to enrich zebrafish DCs by PNA affinity enabled us to use both approaches to further characterize this cell type. We first used histological and histochemical stains to differentiate PNA^{hi} DCs from other leukocytes. Both monocytes and Mφs have been identified in zebrafish by shared characteristics, including high cytoplasmic-to-nuclear ratios and agranular, vacuolated cytoplasm (12, 18, 19). In contrast, PNA^{hi} DCs displayed different morphologies characterized by multiple large dendrites and different body shapes, as revealed by WG and H&E stains (Fig. 3*A*, *i* and *ii*). In addition, PNA^{hi} DCs contained small, acid phosphate (AP)-positive granules that localized perinuclearly, whereas Mφs exhibited larger AP-positive granules that showed a more diffuse cytoplasmic pattern (Fig. 3*A*, *iii*). In mammals, monocytes can be distinguished from granulocytes by α-naphthyl acetate esterase (NAE) staining (20). Here, PNA^{hi} DCs cells stained weakly for NAE compared with monocytic cells, distinguished by a black precipitate throughout the cytoplasm (Fig. 3*A*, *iv*). Neutrophils, eosinophils, and mast cells have been identified in zebrafish by specific staining for myeloperoxidase (MPX), periodic acid-Schiff reagent (PAS), and toluidine blue (TB),

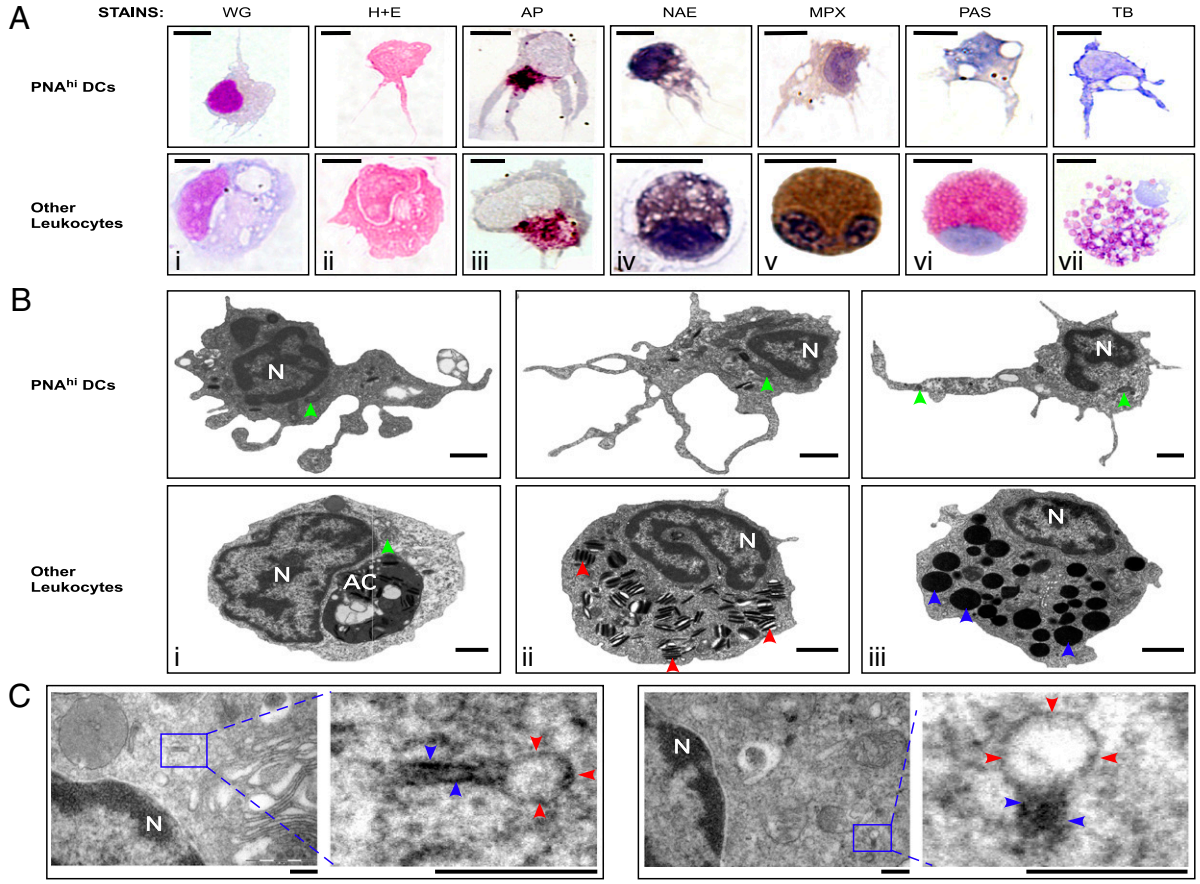

Fig. 3. Morphological characterization of zebrafish DCs. PNA^{hi} myelomonocytes were isolated from WKM (*A* and *B*) or skin (*C*) by FACS. (*A*) Cells were stained for WG, H&E, AP (magenta precipitate), NAE (black precipitate), MPX (brown precipitate), PAS (red precipitate), and TB (purple precipitate). (*Upper*) Putative DCs for each stain. (*Lower*) Positive staining controls: Mφs (*i–iii*), monocyte (*iv*), neutrophil (*v*), eosinophil (*vi*), and mast cell (*vii*). (Scale bar: 5 μm.) (*B*) TEM was performed to examine the ultrastructure of PNA^{hi} myelomonocytes. (*Upper*) DCs. (*Lower*) Other leukocytes: Mφ (*i*), neutrophil (*ii*), and eosinophil (*iii*). Denoted features include nucleus (N), apoptotic corpse (AC), cigar-shaped granules (red arrowheads), round, electron-dense granules (blue arrowheads), and mitochondria (green arrowheads). (Scale bar: 1 μm.) (*C*) TEM analysis of Birbeck-like granules from PNA^{hi} DCs in skin. Magnified granule regions: vacuole (red arrowheads) and rod structure (blue arrowheads). (Scale bar: 200 nm.)

respectively (18, 19, 21). Unlike these granulocyte subsets, the cytoplasm of PNA^{hi} DCs stained negatively for MPX, PAS, and TB (Fig. 3*A*, *v–vii*). Together, these findings suggest that zebrafish PNA^{hi} DCs possess morphological and cytochemical characteristics different from other myeloid cells and reminiscent of those exhibited by mammalian DCs (2, 22).

To examine the ultrastructural properties of zebrafish DCs, we performed transmission electron microscopy (TEM) on PNA^{hi} myelomonocytes purified from WKM. TEM analyses indicated that zebrafish DCs (Fig. 3*B Upper*) possessed many large veils extending from the cell body (measuring 0.5–6 μm in length and 0.1–1 μm in width), some of which contained small and spherical mitochondria. Nuclei tended to be large, contorted, and refractive, with most heterochromatin arranged along the nuclear envelope. Compared with other zebrafish leukocytes (Fig. 3*B Lower*, *i–iii*), DCs display relatively electron lucent cytoplasm, one of the most reliable identifying criteria of mammalian DCs (2). Zebrafish DC cytoplasm contained mitochondria with well-developed cristae, few electron-dense granules or lysosomes, but several translucent vesicles resembling multivesicular bodies or vacuoles. These ultrastructural features match those of classical DCs in mammals (2). Furthermore, we detected the presence of membrane-encapsulated granules that displayed "tennis racket" morphologies in the cytoplasm of PNA^{hi} DCs isolated from skin (Fig. 3*C*). At one end of the granule, a vacuole was often observed containing amorphous, luminal material, whereas the other end was often rod-shaped. Measurements of these granules through the rod-shaped region gave a mean diameter of 37.7 ± 8.59 nm, similar to that of Birbeck granules found in human (45 nm) and murine (43 nm) LCs (23, 24). Considering that Birbeck granules are the morphological markers of mammalian LCs, and that these cells also exhibit PNA binding (15, 16), we postulate that PNA^{hi} DCs isolated from skin are the LC counterpart in zebrafish, supporting the existence of LCs in teleosts, as previously proposed (10).

Further Enrichment of Zebrafish DCs for Functional Analysis. The ability to enrich DCs 70-fold by PNA affinity compared with unfractionated WKM was beneficial, but unfortunately most of these PNA^{hi} cells were neutrophils (60 ± 15%, n = 3; Fig. 2*B*, *i*). To exclude neutrophils from our further analyses, we used transgenic animals that use the myeloperoxidase promoter to drive eGFP expression (*mpx:eGFP*). As shown in Fig. 4*A*, we subfractionated myelomonocytes into Mpx$^-$PNA$^-$, Mpx$^-$PNA$^+$, and Mpx$^+$PNA$^+$. After 4 h of culture to recover dendrite morphology after sorting, analysis of each fraction showed that the Mpx$^+$PNA$^+$ fraction contained 77.8 ± 13.1% neutrophils (Fig. 4*B*, blue text), whereas the Mpx$^-$PNA$^-$ fraction contained mostly erythrocytes (78.1 ± 6.9%; Fig. 4*B*, black text) and erythroid precursor cells (20.2 ± 6.9%). In contrast, the Mpx$^-$PNA$^+$ population contained myeloid precursors (43.9 ± 6.2%; Fig. 4*B*, red text), monocytes (23.9 ± 4.1%), and very few neutrophils

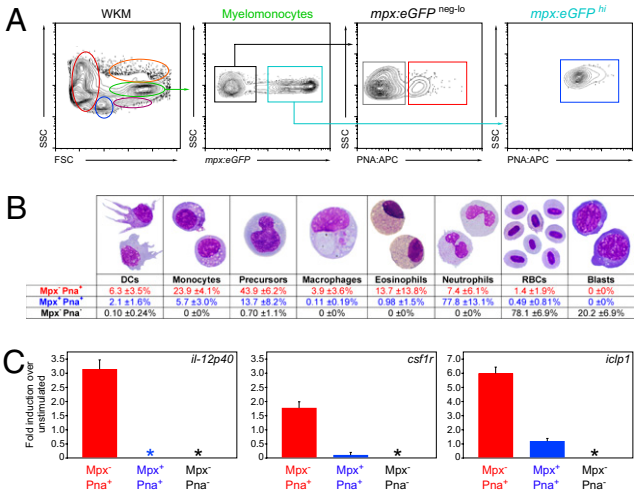

Fig. 4. Further enrichment of zebrafish DCs for functional analyses. (*A*) Single-cell suspensions were prepared from *mpx:eGFP* transgenic WKM and labeled with PNA. Myelomonocytes (green gate) were divided into *mpx*$^-$ (black box) and *mpx*$^+$ (blue box). These populations were further subdivided into *mpx*$^-$ PNA$^-$ (gray box), *mpx*$^-$ PNA$^+$ (red box), and *mpx*$^+$ PNA$^+$ (blue box) fractions. (*B*) After 4 h of culture, *mpx*$^-$ PNA$^-$ (gray), *mpx*$^-$ PNA$^+$ (red), and *mpx*$^+$ PNA$^+$ (blue) fractions were collected and stained with MGG to assess cell morphology. Differentials are presented as mean ± SD, $n = 6$. (*C*) *mpx*$^-$ PNA$^+$ (red bar), *mpx*$^+$ PNA$^+$ (blue bar), and *mpx*$^-$ PNA$^-$ (black bar) myelomonocyte fractions were cultured for 16 h with and without LPS. The abundance of *il-12p40*, *csf1r*, and *iclp1* transcripts were measured by qPCR. Expression is presented as fold induction over nonstimulated controls. Asterisks denote populations with no detectable expression of the transcript. Bars represent mean, $n = 3$. Error bars represent SD.

(7.4 ± 6.1%). Whereas DCs were not proportionally enriched over prior fractionation methods (6.3 ± 3.5%, Fig. 4*B*, compared with 12.8 ± 2.6%, Fig. 2*B*), the total numbers of phenotypic DCs collected were over 500-fold enriched vs. unfractionated WKM. Importantly for functional studies, Mφs, which are also APCs, were significantly reduced (3.9 ± 3.6%, Fig. 4*B*, compared with 10.0 ± 3.5%, Fig. 2*B*, *iii*). After stimulating each purified fraction with *E. coli* LPS, the Mpx$^-$PNA$^+$ population uniquely up-regulated *il-12p40*, an essential cytokine for T-helper cell differentiation and NK activation (Fig. 4*C Left*, red bar). In mammals, IL-12 expression can be induced in Mφs and other myeloid cells, but is mainly produced by DCs in response to antigenic stimulation, when its p40 subunit is up-regulated (25). In addition, Mpx$^-$PNA$^+$ cells up-regulated *csf1r* (Fig. 4*C Center*, red bar), an essential growth factor receptor found on mammalian DCs, as well as the MHC class II invariant chain *iclp1* (Fig. 4*C Right*, red bar), an essential component of exogenous antigen presentation that is constitutively expressed by all APCs, including B cells, Mφs, and DCs (26), whereas the other myelomonocyte fractions were unresponsive to LPS-mediated gene induction (Fig. 4*C*, blue and gray bars).

Functional Characterization of DC-Enriched Populations. As shown in Fig. 1, we detected zebrafish DCs based upon their phagocytic ability. We next asked whether this assay, in combination with PNA affinity, could be used to further characterize these cells. Following peritoneal injection of Alexa 488-labeled *S. aureus*, we collected IPEX and stained the cell samples with PNA for FACS analysis. Though not all myeloid PNA^{hi} cells phagocytosed *S. aureus* (Fig. 5*A Upper*, blue gate), all phagocytes (7.5 ± 1.7%, $n = 4$) were PNA^{hi} (green gate). PNA$^-$ cells (Fig. 5*A Upper*, red gate) were not phagocytic. We subjected each purified cell population to qPCR analyses to determine the expression of the activation-induced *il12p40* gene. Though expression of *il-12p40* was not detectable in PNA$^-$ myelomonocytes (Fig. 5*A Lower*, red bar), it was detected in PNA^{hi} nonphagocytes at approximately half the levels of that in WKM (blue bar). By contrast, *il-12p40* expression in PNA^{hi} phagocytes showed an approximate 18-fold increase compared with that in WKM (Fig. 5*A Lower*, green bar). Cytospin analyses of these three populations revealed that DCs were twice as abundant within purified PNA^{hi} phagocytes (9.9 ± 1.3%, $n = 3$) compared with the PNA^{hi} nonphagocytic fraction (5.1 ± 0.7%, $n = 3$). DCs were rare within purified PNA$^-$ cells (0.2 ± 0.3%, $n = 3$). These data confirm that PNA^{hi} phagocytes express relatively high levels of *il-12p40* transcripts, and suggest that DCs within this population may contribute to the expression of this important inflammatory cytokine.

Zebrafish PNA^{hi} Myelomonocytes Stimulate T Cells in an Antigen-Dependent Manner. In mammals, DCs are widely accepted as the most potent and versatile APC due to their ability to prime naïve T cells both in vitro and in vivo (26). This reputation as professional APCs derives from early studies in which DC-enriched populations were shown to be powerful stimulators of the mixed leukocyte reaction and in a number of antigen-specific T-helper responses (6). To enable similar functional assays in the zebrafish, we sought to develop assays to test APC function. We therefore performed immunization studies in adult *lck:eGFP* transgenic zebrafish using keyhole limpet hemocyanin (KLH), a well-known soluble protein that promotes a polyclonal T-cell response in both mammals and teleosts (27, 28). As previously demonstrated, the zebrafish leukocyte-specific protein tyrosine kinase (*lck*) gene promoter drives GFP expression in T lymphocytes, making this transgenic line an ideal source to isolate KLH-primed T cells (T_{KLH}) after immunization (29). We immunized *lck:eGFP* animals by i.p. injection of KLH emulsified in complete Freund's adjuvant to induce a general inflammatory response, followed 2 wk later by a second i.p. injection with KLH emulsified in incomplete Freund's adjuvant to boost the T-cell response against this soluble protein (see Fig. 5*B*). Control animals were immunized with adjuvant alone to isolate "naive" lck$^+$ T cells (T_{naive}). Five days after boosting, lck$^+$ T_{KLH} and lck$^+$ T_{naive} cell subsets were isolated from the gut, spleen, and peritoneal cavity by FACS (at a purity of ≥95% based on GFP expression), and labeled with the red membrane dye PKH26 to permit detection of cell proliferation through stepwise loss of dye signal. Subsequently, each T-cell subset was cultured in the presence of purified PNA^{hi} myelomonocytes either pulsed (loaded) or not (unloaded) with KLH. Because pure inbred zebrafish lines do not exist due to infertility resulting from successive inbreeding (11), we isolated myelomonocytes from the WKM of the same *lck:eGFP* animals immunized to lessen allogeneic responses. After 3 days of coculture, cells were harvested and the proliferation of lck$^+$ T cells was measured by flow cytometry. As shown in Fig. 5*C*, primed T cells (T_{KLH}) proliferated over 3-fold more when exposed to KLH-loaded PNA^{hi} cells (Fig. 5*C Upper*) vs. KLH-loaded PNA$^-$ cells (Fig. 5*C Lower*) isolated from the myelomonocyte fraction, supporting our conclusion that zebrafish APCs are highly enriched within the PNA^{hi} myeloid fraction. To further examine the ability of PNA^{hi} cells to stimulate proliferation in response to specific antigen, primed T cells were exposed to PNA^{hi} cells loaded with KLH (Fig. 5*D Upper*) or not (Fig. 5*D Lower*). As KLH-loaded APCs led to an approximately 3-fold increase in proliferation compared with unloaded APCs, this experiment demonstrated that the T-cell proliferation was antigen specific. As expected, primed T cells (Fig. 5*E Upper*) proliferated more readily than naïve T cells (Fig. 5*E Lower*), suggesting that the marked survival and proliferation increases observed were due to prior, in vivo stimulation of KLH-responsive T-cell clones by PNA^{hi} APCs. Together, these findings show that the PNA^{hi} myeloid fraction of WKM contains APCs able to uptake, process, and present antigen to stimulate proliferation of T lymphocytes in an antigen-dependent manner.

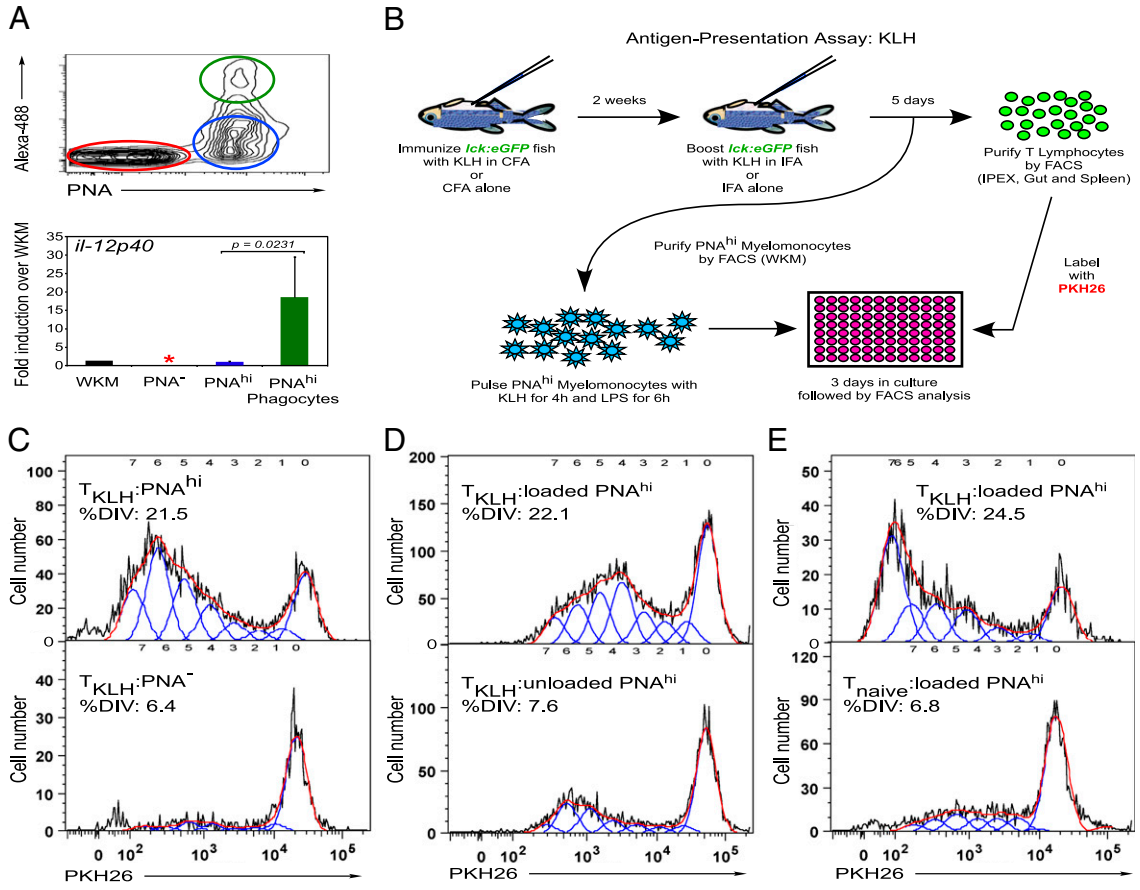

Fig. 5. Functional characterization of Zebrafish DC-enriched populations. (*A Upper*) In vivo phagocytosis by PNA^{hi} myelomonocytes. *S. aureus* Alexa 488 was injected i.p., and 16 h later cells were collected from IPEX, stained with PNA, and analyzed by FACS. Cells were gated on the myelomonocyte gate and divided into the following populations: PNA^{-} (red gate and bar), PNA^{hi} (blue gate and bar), and PNA^{hi} phagocytes (green gate and bar). (*Lower*) qPCR analysis of *il-12p40* transcript in these populations relative to that in WKM (black bar, arbitrary unit set at 1). Data are shown as average of fold change over WKM ± SD (n = 4). Asterisk indicates transcript not detected. (*B*) Illustration of the antigen-presentation assay using KLH to prime a polyclonal T-cell response, with the *lck:eGFP* zebrafish transgenic line as the source for naive (T_{naive}) or KLH-primed (T_{KLH}) T lymphocytes. (*C*) Proliferation responses as measured by dilution of PKH26 of *lck*$^{+}$-T_{KLH} cells stimulated with either PNA^{hi} (*Upper*) or PNA^{-} (*Lower*) myelomonocytes loaded with KLH protein. (*D*) *lck*$^{+}$-T_{KLH} cells stimulated with PNA^{hi} myelomonocytes loaded (*Upper*) or not loaded (*Lower*) with KLH. (*E*) *lck*$^{+}$-T_{KLH} (*Upper*) or *lck*$^{+}$-T_{naive} (*Lower*) cells stimulated with PNA^{hi} myelomonocytes loaded with KLH. T-cell proliferation results (*C–E*) are representative of three independent experiments. For all proliferation assays, the APC/T-cell ratio = 5:1. Histograms show T-cell proliferation as modeled by the FlowJo proliferation tool. %DIV = percent of T cells that divided.

In seeking to describe antigen-presenting cells in zebrafish, we have identified and characterized DCs in this animal model. Our findings suggest that DCs were present in the ancestor common to teleosts and mammals, and that this key link between the innate and adaptive immune systems has been in place for over 450 million years. These studies lay the foundation for future work aimed at understanding antigen presentation and immune responses in the zebrafish. Our findings also suggest that creation of transgenic animals harboring fluorescent reporters under control of the *il-12* or *mhcII* promoters will be useful to specifically mark APCs to directly monitor the early immune response in living animals. Our establishment of an immunization protocol to prime a zebrafish T-cell response in vivo will enable more-refined prospective isolation approaches, APC-derived vaccinations, vaccinations against specific pathogens, and more detailed analyses of APC function. With continued efforts to generate transgenic lines specifically marking each hematopoietic lineage, our assay to test APC function will permit the identification and efficacy of each APC subset in the activation of the specific immune response in the zebrafish.

Materials and Methods

Zebrafish Stocks and Embryos. Zebrafish were mated, staged, and raised as previously described, and maintained in accordance with University of California, San Diego, Institutional Animal Care and Use Committee guidelines (12). *Tg(lck:eGFP)cz1* (29) and *Tg(mpx:eGFP)i114* (30) transgenic zebrafish were used.

Cell Preparation. Single-cell suspensions of WKM were prepared from adult zebrafish as previously described (31). IPEX cells were collected after making a ventral incision and washing the peritoneal cavity with PBS (Mediatech, Inc.). Skin samples were prepared by dissociating 1 cm^2 sections of skin in PBS with Liberase Blendzyme II according to manufacturer's instructions (Roche), followed by subsequent filtration. Single-cell suspensions from other organs were prepared by manual trituration and filtration. Cells were counted with a hemocytometer (Hausser Scientific), and viability was assessed by Trypan Blue (Invitrogen) exclusion.

Flow Cytometry and Sorting. After single-cell suspensions were prepared from WKM, they were stained with biotinylated peanut agglutinin (PNA; Vector Laboratories) and allophycocyanin-conjugated (APC) streptavidin (eBioscience). Dead cells were excluded by propidium iodide positivity. Cells were analyzed and sorted with a LSR-II and FACSAria I (both BD Biosciences), respectively. Flow cytometry data were analyzed with FlowJo software (TreeStar). For in vivo phagocytosis assay, 2 μg of *S. aureus* conjugated to Alexa 488 fluorophore (Molecular Probes) was injected i.p. (1 mg/mL). Cells were collected from the IPEX 16 h after injection for analysis.

Cytology. After purified myelomonocyte populations were cultured (2 × 10^4 cells/well) in a 96-well plate (Corning Inc.) with complete media (32) for 4 h,

cells were harvested and cytospins were performed as previously described (31–34) using a Shandon Cytospin 4 (Thermo Fisher Scientific). Cells were fixed and stained with H&E (Thermo Fisher Scientific), WG, May-Grünwald Giemsa (MGG), MPX, PAS, TB, or NAE according to the manufacturer's instructions (all from Sigma). For in vitro induction of gene expression, purified myelomonocyte fractions were cultured for 16 h with the addition of PBS or *E. coli* LPS (1 μg/mL).

Microscopy. Cytospins were imaged using a DP70 microscope (Olympus America). For transmission electron microscopy (TEM), cells were fixed in 3% glutaraldehyde in 0.1 M cacodylate buffer, centrifuged, and washed in 0.1 M cacodylate buffer. Cells were embedded in 12% gelatin/PBS and centrifuged to reform a pellet in a microfuge tube. The gelatin/pellets were cut out of the microfuge tubes, postfixed in buffered 1% osmium tetroxide, buffer washed, dehydrated in a graded ethanol series, and transitioned through propylene oxide. The samples were embedded in Embed 812/Araldite (Electron Microscopy Sciences). Thin (60 nm) sections of the pellets were cut, mounted on parlodion-coated copper slot grids, and stained with uranyl acetate and lead citrate for examination on a Philips CM100 electron microscope (Philips/FEI Corporation) at 80 kV. Images were documented by using a MegaView III charge-coupled device camera (Olympus America) and converted to TIF format for subsequent processing in Adobe Photoshop.

Quantitative PCR (qPCR). RNA was obtained using RNeasy Protect (Qiagen). cDNA was prepared from RNA with random hexamer qScript Supermix (Quanta BioSciences) and controlled for contamination with separate reactions lacking reverse transcriptase. qPCR reactions were performed in triplicate with SsoFast EvaGreen Mastermix (Bio-Rad) and quantitated on the CFX96 system (Bio-Rad) using the ΔΔCt method with *ef1α* (35) as a reference gene. Product sizes of qPCR reactions were confirmed by gel electrophoresis. Primers were designed with Primer3 software: *il-12p40* (gene id: ENSDARG00000033727) forward: GATACCCAGACTCCTGGAAC; reverse: GAGACTTTGTGTGCGGTAAG; *csfr1* (gene id: ENSDARG00000007889) forward: ATGACCATACCCAACTTTCC; reverse: AGTTTGTTGGTCTGGATGTG; and *iclp1* (gene id: ENSDARG00000009087) forward: AGAAGCAGCACATCAACG; reverse: AAGTGGGGTCAGAGTAATCC.

Antigen Presentation Assay. *lck:eGFP* animals were immunized by i.p. injection with 2 μg of KLH (Sigma) emulsified in complete Freund's adjuvant (CFA, 1 mg/mL; Sigma), followed 2 wk later by a second injection with 2 μg of KLH emulsified in incomplete Freund's adjuvant (IFA, 1 mg/mL; Sigma). Control fish were immunized with adjuvant alone to isolate "naive" lck^+-T cells (T_{naive}). Five days after boosting, lck^+-T_{KLH} cells were isolated from the gut, spleen, and peritoneal cavity by FACS (at a purity of ≥95% based on GFP expression), labeled with the membrane dye PKH26 (Sigma), and cultured (5×10^4 cells/well) in a 96-well plate (Corning Inc.). T cells were then challenged with PNA^{hi} myelomonocytes (APC/T-cell ratio = 5:1) isolated from the WKM of the same *lck:eGFP* animals that had been cultured with KLH protein (100 μg/mL) for 4 h, and stimulated with *E. coli* LPS (1 μg/mL) for an additional 6 h. After 3 d of coculture, cells were harvested, and the proliferation of lck^+-T cells was measured by flow cytometry. The FlowJo proliferation tool was used to analyze the division-mediated dilution of PKH26 fluorescence in *lck*:$eGFP^+$ T cells. Percentage of T cells that divided (%DIV) was calculated by FlowJo's proliferation wizard software.

Statistics. Data were analyzed with the two-tailed Student's *t* test. Differences were deemed significant at $P < 0.05$.

ACKNOWLEDGMENTS. We thank A. J. Feeney, A. W. Goldrath, D. M. Page, B. Santoso, and E. Zuñiga for critical evaluation of the manuscript, Malcolm Wood for TEM analyses, V. Wittamer (University of California, La Jolla, CA) for providing the *il-12p40, csf1r,* and *iclp1* primers, Roger Rainville, Evie Wright, and Lisa Phelps for excellent animal care, Karen Ong for support on cell purification by FACS, and Kerstin Richter for excellent laboratory management. This work was supported by National Institute of Diabetes and Digestive and Kidney Diseases Research Supplement Fellowship 3R01DK074482-01 (to G.L.-V.), San Diego Institutional Research and Academic Career Development Award Fellowship GMO68524 (to G.L-V.), National Research Service Award T32-HL086344 (to D.L.S.), University of California, San Diego CURE Grant 5P30CA23100-22S2 (to K.B.), the American Society of Hematology (D.T.), the Senyei Family Foundation (D.T.), and National Institutes of Health Grant R01-DK074482 (to D.T.).

1. Jolles S (2002) Paul Langerhans. *J Clin Pathol* 55:243.
2. Steinman RM, Cohn ZA (1973) Identification of a novel cell type in peripheral lymphoid organs of mice. I. Morphology, quantitation, tissue distribution. *J Exp Med* 137:1142–1162.
3. Steinman RM, Cohn ZA (1974) Identification of a novel cell type in peripheral lymphoid organs of mice. II. Functional properties in vitro. *J Exp Med* 139:380–397.
4. Steinman RM, Lustig DS, Cohn ZA (1974) Identification of a novel cell type in peripheral lymphoid organs of mice. 3. Functional properties in vivo. *J Exp Med* 139: 1431–1445.
5. Steinman RM, Adams JC, Cohn ZA (1975) Identification of a novel cell type in peripheral lymphoid organs of mice. IV. Identification and distribution in mouse spleen. *J Exp Med* 141:804–820.
6. Steinman RM (2007) Dendritic cells: Understanding immunogenicity. *Eur J Immunol* 37(Suppl 1):S53–S60.
7. Miranda de Carvalho C, Bonnefont-Rebeix C, Rigal D, Chabanne L (2006) Dendritic cells in different animal species: An overview. *Pathol Biol (Paris)* 54:85–93.
8. Du Pasquier L (2005) Meeting the demand for innate and adaptive immunities during evolution. *Scand J Immunol* 62(Suppl 1):39–48.
9. Rombout JH, Huttenhuis HB, Picchietti S, Scapigliati G (2005) Phylogeny and ontogeny of fish leucocytes. *Fish Shellfish Immunol* 19:441–455.
10. Lovy J, Wright GM, Speare DJ (2008) Comparative cellular morphology suggesting the existence of resident dendritic cells within immune organs of salmonids. *Anat Rec (Hoboken)* 291:456–462.
11. Trede NS, Langenau DM, Traver D, Look AT, Zon LI (2004) The use of zebrafish to understand immunity. *Immunity* 20:367–379.
12. Traver D, et al. (2003) Transplantation and in vivo imaging of multilineage engraftment in zebrafish bloodless mutants. *Nat Immunol* 4:1238–1246.
13. Sharon N (1983) Lectin receptors as lymphocyte surface markers. *Adv Immunol* 34: 213–298.
14. El Sherbini H, et al. (2000) Lectin ligands on human dendritic cells and identification of a peanut agglutinin positive subset in blood. *Cell Immunol* 200:36–44.
15. Nakamura K, Ishii A, Tamaki K (1990) Subpopulation of murine epidermal Langerhans cells identified by lectin-binding sites. *Arch Dermatol Res* 282:253–257.
16. Schuler G, Romani N, Linert J, Shevach EM, Stingl G (1983) Subsets of epidermal Langerhans cells as defined by lectin binding profiles. *J Invest Dermatol* 81:397–402.
17. Inaba K, et al. (1992) Generation of large numbers of dendritic cells from mouse bone marrow cultures supplemented with granulocyte/macrophage colony-stimulating factor. *J Exp Med* 176:1693–1702.
18. Bennett CM, et al. (2001) Myelopoiesis in the zebrafish, Danio rerio. *Blood* 98: 643–651.
19. Lieschke GJ, Oates AC, Crowhurst MO, Ward AC, Layton JE (2001) Morphologic and functional characterization of granulocytes and macrophages in embryonic and adult zebrafish. *Blood* 98:3087–3096.
20. Yam LT, Li CY, Crosby WH (1971) Cytochemical identification of monocytes and granulocytes. *Am J Clin Pathol* 55:283–290.
21. Dobson JT, et al. (2008) Carboxypeptidase A5 identifies a novel mast cell lineage in the zebrafish providing new insight into mast cell fate determination. *Blood* 112: 2969–2972.
22. Zarnani AH, et al. (2006) The efficient isolation of murine splenic dendritic cells and their cytochemical features. *Histochem Cell Biol* 126:275–282.
23. Grassi F, et al. (1998) Monocyte-derived dendritic cells have a phenotype comparable to that of dermal dendritic cells and display ultrastructural granules distinct from Birbeck granules. *J Leukoc Biol* 64:484–493.
24. Pérez-Torres A, Ustarroz-Cano M (2001) Demonstration of birbeck (Langerhans cells) granules in the normal chicken epidermis. *J Anat* 199:493–497.
25. Lyakh L, Trinchieri G, Provezza L, Carra G, Gerosa F (2008) Regulation of interleukin-12/interleukin-23 production and the T-helper 17 response in humans. *Immunol Rev* 226:112–131.
26. Banchereau J, et al. (2000) Immunobiology of dendritic cells. *Annu Rev Immunol* 18: 767–811.
27. Marrack PC, Kappler JW (1975) Antigen-specific and nonspecific mediators of T cell/B cell cooperation. I. Evidence for their production by different T cells. *J Immunol* 114: 1116–1125.
28. Miller NW, Clem LW (1984) Temperature-mediated processes in teleost immunity: Differential effects of temperature on catfish in vitro antibody responses to thymus-dependent and thymus-independent antigens. *J Immunol* 133:2356–2359.
29. Langenau DM, et al. (2004) In vivo tracking of T cell development, ablation, and engraftment in transgenic zebrafish. *Proc Natl Acad Sci USA* 101:7369–7374.
30. Renshaw SA, et al. (2006) A transgenic zebrafish model of neutrophilic inflammation. *Blood* 108:3976–3978.
31. Stachura DL, Traver D (2009) *Essential Zebrafish Method: Cell and Developmental Biology* (Academic/Elsevier Life Sciences, San Diego).
32. Stachura DL, et al. (2009) Zebrafish kidney stromal cell lines support multilineage hematopoiesis. *Blood* 114:279–289.
33. Bertrand JY, et al. (2007) Definitive hematopoiesis initiates through a committed erythromyeloid progenitor in the zebrafish embryo. *Development* 134:4147–4156.
34. Bertrand JY, Cisson JL, Stachura DL, Traver D (2010) Notch signaling distinguishes 2 waves of definitive hematopoiesis in the zebrafish embryo. *Blood* 115:2777–2783.
35. Bertrand JY, Kim AD, Teng S, Traver D (2008) CD41+ cmyb+ precursors colonize the zebrafish pronephros by a novel migration route to initiate adult hematopoiesis. *Development* 135:1853–1862.